Int. J. Heat Mass Transfer. Vol. 16, pp. 311–328. Pergamon Press 1973. Printed in Great Britain

EXPERIMENTS ON A SHROUDED, PARALLEL DISK SYSTEM WITH ROTATION AND COOLANT THROUGHFLOW

J. P. YU, E. M. SPARROW and E. R. G. ECKERT

Department of Mechanical Engineering, University of Minnesota, Minneapolis, Minnesota 55455, U.S.A.

(*Received* 13 *January* 1972 *and in revised form* 8 *May* 1972)

Abstract— The heat transfer and fluid flow characteristics of a cylindrical enclosure having both rotating and stationary walls have been investigated in the presence of coolant throughflow. The research was motivated by cooling applications in cavities and enclosures which may be situated adjacent to the rotating shaft in gas turbines, compressors, and similar devices. The test section walls consisted of a heated rotating disk, a heated stationary cylindrical shroud, and an insulated stationary disk. The coolant passing through the enclosure was air. The experiments were performed over a range of disk rotational speeds, coolant flow rates and spacings between the disks.

The local heat transfer coefficients on the rotating disk were found to increase with increasing rotational speed, increasing coolant flow rate, and decreasing spacing. The shapes of the radial distributions of the transfer coefficients suggested the existence of laminar, transition, and turbulent regimes. In the laminar regime, the transfer coefficients were relatively insensitive to the coolant flow rate. For the shroud, the trends with rotational speed, coolant flow, and spacing were generally similar to those for the rotating disk. However, owing to backflows along the shroud at the lower rotational speeds, the trends were more complex in that range. Flow visualization, accomplished by smoke injection, revealed a succession of flow patterns which could be ordered according to the ratio of the coolant flow rate to the disk rotational speed.

NOMENCLATURE

A, surface area;
h, local heat transfer coefficient, equation (1);
$\bar{h}$, average heat transfer coefficient, equation (4);
k, thermal conductivity;
$\dot{m}$, coolant mass flow rate;
Q, overall heat transfer rate;
q, local heat transfer rate per unit area;
R, radius of enclosure;
R_i, radius of inlet pipe;
r, radial coordinate;
Re_i, coolant inlet Reynolds number, equation (2);
$Re_{\omega,R}$, disk rotational Reynolds number, equation (2);
s, spacing between disks;
T_w, local wall temperature;
T_f, coolant inlet bulk temperature;
x, axial coordinate measured from rotating disk;
μ, viscosity;
ν, kinematic viscosity;
ω, disk rotational speed.

INTRODUCTION

THE RESEARCH described in this paper is motivated by cooling problems encountered in gas turbines, compressors, and other rotating devices. These devices may contain cavities and enclosures of various shapes and sizes situated adjacent to the rotating shaft. Some or all of the walls which bound such enclosures may be rotating. The walls may be heated by conductive, convective, or radiative transport from regions of high temperature, for instance, from the combustion chamber or turbine blades. One practical approach to the cooling of the walls is to pass a relatively low temperature air stream

(e.g. bleed air) through the enclosure, either from a duct in the hollow shaft or from an annular duct which surrounds the shaft.

The present experiments were undertaken to provide basic heat transfer information appropriate to the applications discussed in the preceding paragraph. In addition, fluid flow patterns were investigated using a flow visualization technique.

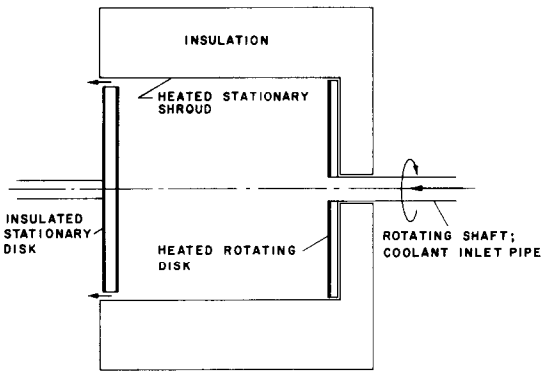

FIG. 1. Test section schematic.

The test section that was employed in the heat transfer experiments is shown schematically in Fig. 1. It consisted, in essence, of a cylindrical enclosure bounded by a heated rotating disk, an insulated stationary disk, and a heated stationary cylindrical shroud. The coolant air stream entered the enclosure through an aperture situated at the center of the rotating disk and exited through an annular gap adjacent to the rim of the stationary disk. The spacing between the disks could be changed at will. The thermal boundary condition on the heated surfaces was designed to be uniform heat flux.

The parameters that were varied during the course of the experiments included the disk rotational speed (500–3700 rpm), the flow rate of the coolant air (inlet pipe Reynolds numbers from 15 000 to 68 000), and the spacing between the disks (spacing to radius ratios from 0·22 to 2). The fact that relatively large spacing to radius ratios were investigated is a noteworthy departure from most prior studies of rotating disk systems. Such studies were generally motivated by applications involving turbine disks and were, therefore, concerned with relatively small spacing to radius ratios.

A survey of the literature failed to unearth any prior experiments on heat transfer in shrouded, parallel disk systems with rotation and coolant throughflow. The only instance of a configuration which somewhat resembles that of Fig. 1 was the one employed by Bayley and Owen [1], who were concerned solely with fluid flow aspects. In that apparatus, the coolant entered the enclosure via a central aperture in the stationary disk and exited by passing radially outward through a clearance between the rotating disk and the shroud. The largest value of the spacing to radius ratio was 0·18. Hennecke and co-workers [2] have solved for the laminar flow and heat transfer in a rotating cylindrical enclosure with coolant entering via a central aperture in one disk and exiting through a similar aperture in the other disk. Investigations dealing with unshrouded, parallel disk systems with coolant throughflow are described in [3–10], whereas shrouded systems without coolant throughflow are investigated in [11–14].

A more detailed literature survey is available in the thesis [15] on which this paper is based. Also available in [15] are details relating to apparatus design and fabrication, instrumentation, experimental technique, data reduction and correlation, and error analysis.

EXPERIMENTAL APPARATUS

The test section, shown schematically in Fig. 1, comprised only one part of the overall apparatus that was designed and fabricated for the experiments. The remainder of the system can be outlined by following the coolant air stream on its course of flow. The air, supplied by a laboratory compressed air system, successively passed through a filter, a flow control device, a calibrated square-edged metering orifice, and a heat exchanger whose function was to cool the air.

From the heat exchanger, the air stream was piped into a plenum chamber, which was situated at the upstream end of the hollow rotating shaft pictured at the right in Fig. 1. The air then passed into the shaft via a circumferential array of narrow longitudinal slots and flowed toward the test section. The internal diameter of the rotating shaft was 2 in. (5·1 cm) and its length–diameter ratio was 22.

The components of the test section will now be described. The diameters of the rotating disk, stationary disk, and cylindrical shroud were $17\frac{3}{4}$, 17 and 18 in. (45·1, 43·2 and 45·7 cm), respectively. The maximum separation distance between the disks was 18 in. (45·7 cm), and the minimum separation at which data runs were made was 2 in. (5·1 cm). The diameter of the coolant inlet aperture, 2 in. (5·1 cm), was selected to be about $\frac{1}{10}$ of the disk diameter in accordance with the practice that such apertures be relatively small. The annular gap of $\frac{1}{2}$ in. (1·3 cm) for fluid outflow at the rim of the stationary disk was chosen small enough so that its size would not affect the flow field in the enclosure proper.

The rotating disk was a composite structure consisting of a $\frac{3}{4}$ in. (1·9 cm) thick backing layer of Benelex 401 (a pressed wood product) and a 0·029 in. (0·074 cm) thick stainless steel surface plate, with bonding being accomplished by a high thermal conductivity, low electrical conductivity epoxy. The choice of Benelex as the thermally insulating backing material was based on its low thermal conductivity, high tensile strength, low density, low moisture absorption, and easy machinability. On the front face of the Benelex (adjacent to the surface plate), 150 concentric grooves were machined, into which an electrical resistance heating wire was coiled and embedded.

The function of the surface plate was to smooth the heat flux distribution provided by the discrete turns of heating wire, to present a hydrodynamically smooth surface to the flow, and to facilitate temperature measurement. Stainless steel was chosen as the surface plate material because its coefficient of thermal expansion is nearly equal to that of Benelex and because of its near immunity to surface damage during the fabrication process. The thickness of the surface plate was selected on the basis of finite-difference solutions of the heat conduction equation, taking account of radial and axial conduction in the plate.

Surface temperature measurements for the rotating disk were accomplished by means of miniaturized calibrated thermistors embedded in the stainless steel surface plate. Ten thermistors were installed along a radial line, and three thermistors were distributed circumferentially at 90 degree intervals to provide a check on axial symmetry. It was demonstrated by finite-difference computations that the presence of the thermistors would have a negligible effect on the surface temperature. In addition, to facilitate heat loss estimates, three thermistors were embedded in the rear face of the Benelex backing plate. The use of thermistors for the rotating disk temperature measurements was dictated by the contact resistance inherent in the slip rings which convey electrical signals from rotating to stationary members.

The stationary cylindrical shroud was fabricated by forming and butt welding a 0·025-in. (0·064 cm) thick stainless steel sheet. On the convex surface of the cylinder, thirty roll-calibrated, copper–constantan thermocouples were soldered along a horizontal line. Another twelve thermocouples were installed at other locations to check on axial symmetry. The cylinder was then wrapped with insulating tape and electrical resistance heating ribbon. To provide thermal insulation and the necessary stiffness and rigidity, a thick layer of polyurethane foam was molded on the outside of the cylinder. Within the foam layer, six thermocouples were installed to facilitate heat loss estimates.

Special wiring arrangements were made for the shroud heater in order to accommodate different separation distances between the stationary and rotating disks. The heater was designed for separation distances of 18, 12, 8, 4

and 2 in. (45·7, 30·5, 20·3, 10·2 and 5·1 cm). For each of these, provision was made for a main heating section which spanned an axial length equal to the separation distance, plus flanking guard heaters for minimizing end losses.

As seen in Fig. 1, the insulating layer of polyurethane foam also extended behind the rotating disk. The thermal conductivity of the foam is about 30 per cent less than that of air.

The stationary disk was of sandwich construction, with front and rear plates of textolite and polyurethane foam as filler. Along the outer rim, the textolite plates were separated by a ring of Plexiglas. Nineteen thermocouples were installed in the stationary disk, and these were used to estimate heat losses. The stationary disk was supported by a shaft and frame assembly which was mounted on a lathe bed to facilitate its axial movement. The separation distance between the disks was changed by changing the axial position of the stationary disk.

To measure the exit temperature of the coolant air, thermocouples were installed in the annular gap between the stationary disk and the shroud, in the plane of the front face of the disk. In each of four circumferential locations (90 degrees apart), three thermocouples were distributed across the section of the gap. Coolant exit temperatures were actually measured at eight circumferential locations, the additional four locations being attained by a 45 degree rotation of the stationary disk.

The rotating members of the system were driven by a variable speed motor which provided a continuous variation over the range from 420 to 3750 rpm. The rotating shaft had been dynamically balanced prior to the attachment of the disk, and the shaft-disk system was subsequently dynamically balanced as a unit. Even at 3700 rpm, which was the highest rotational speed of the tests, the system operated at a remarkably low noise level and was free of obvious vibrations.

All measurements were made with laboratory grade instruments which, wherever possible, had been checked or calibrated against standards.

FLOW VISUALIZATION STUDIES

Flow visualization studies, performed as a complement to the heat transfer experiments, will now be described. To facilitate the visualization, a transparent cylindrical shroud and transparent stationary disk were installed in place of their heat transfer counterparts. A number of techniques was explored in an attempt to visualize the flow [15] and, of these, smoke appeared to give the best results. High rates of sustained smoke generation were required because of the highly disturbed nature of the flow, the relatively large physical dimensions of the apparatus, and the long-time viewing needed to observe the complex flow patterns. This requirement, along with limitations with respect to flammability and toxicity, motivated the development of a new smoke generator, which is described elsewhere [16].

The smoke was introduced into the enclosure through twenty-six, $\frac{3}{16}$ in. (0·48 cm) dia. injection holes. Eighteen of the holes were located in the shroud, distributed axially along a horizontal line. There were seven injection holes distributed along a radial line on the front face of the stationary disk, and a single hole on the rim of the disk. With all twenty-six holes in use, the smoke generator provided sufficient smoke for about 25 min of continuous viewing.

Results from the flow visualization studies will be presented in two stages. First, representative flow field photographs will be exhibited and, subsequently, sketches of the flow patterns will be given.

The flow field photographs are contained in Figs. 2 and 3, respectively for disk rotational speeds of 3000 and 500 rpm. All photographs are for a spacing to radius ratio of 2. In each photograph, the coolant air enters at the right (as in Fig. 1). The entering coolant is free of smoke and, therefore, appears as a dark region in the photographs.

Consideration is first given to Fig. 2. The figure has three columns of photographs which correspond, from left to right, to coolant inlet Reynolds numbers Re_i of 15 000, 25 000 and

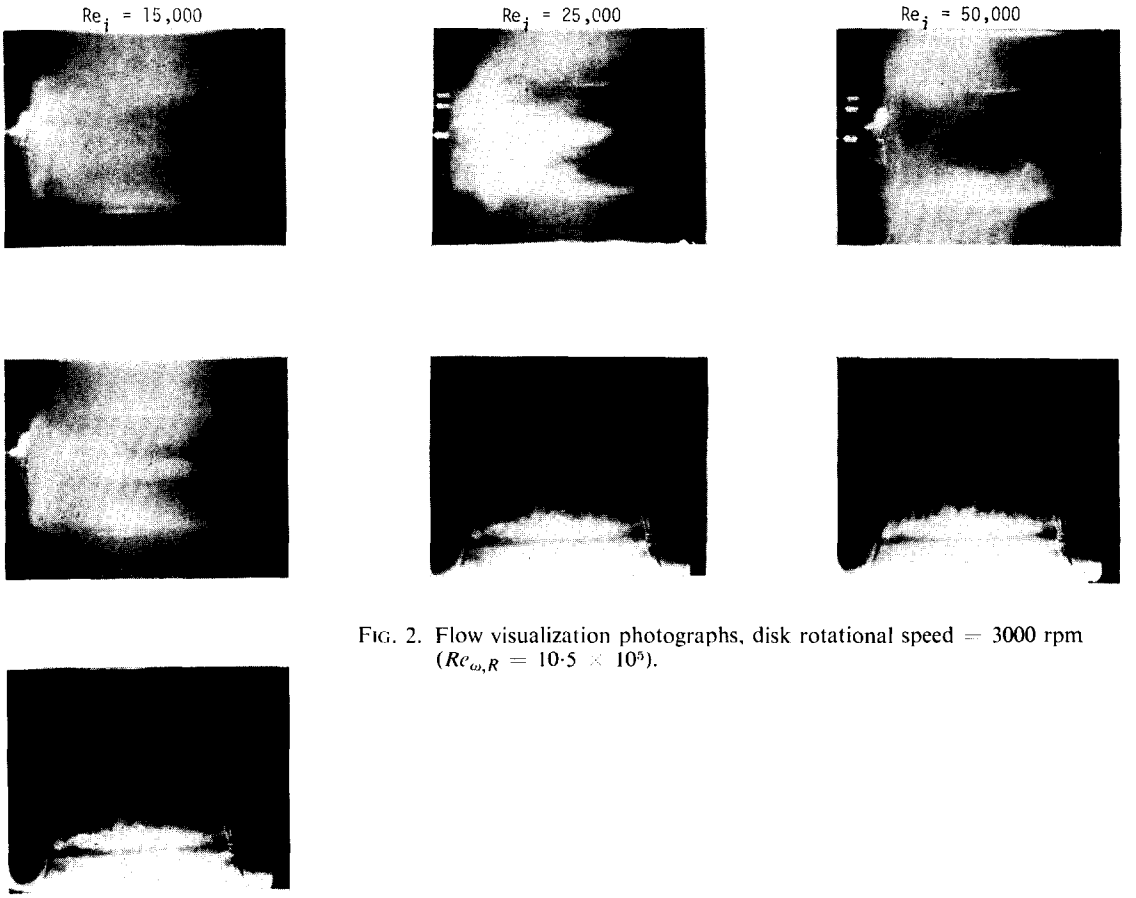

FIG. 2. Flow visualization photographs, disk rotational speed = 3000 rpm ($Re_{\omega,R} = 10{\cdot}5 \times 10^5$).

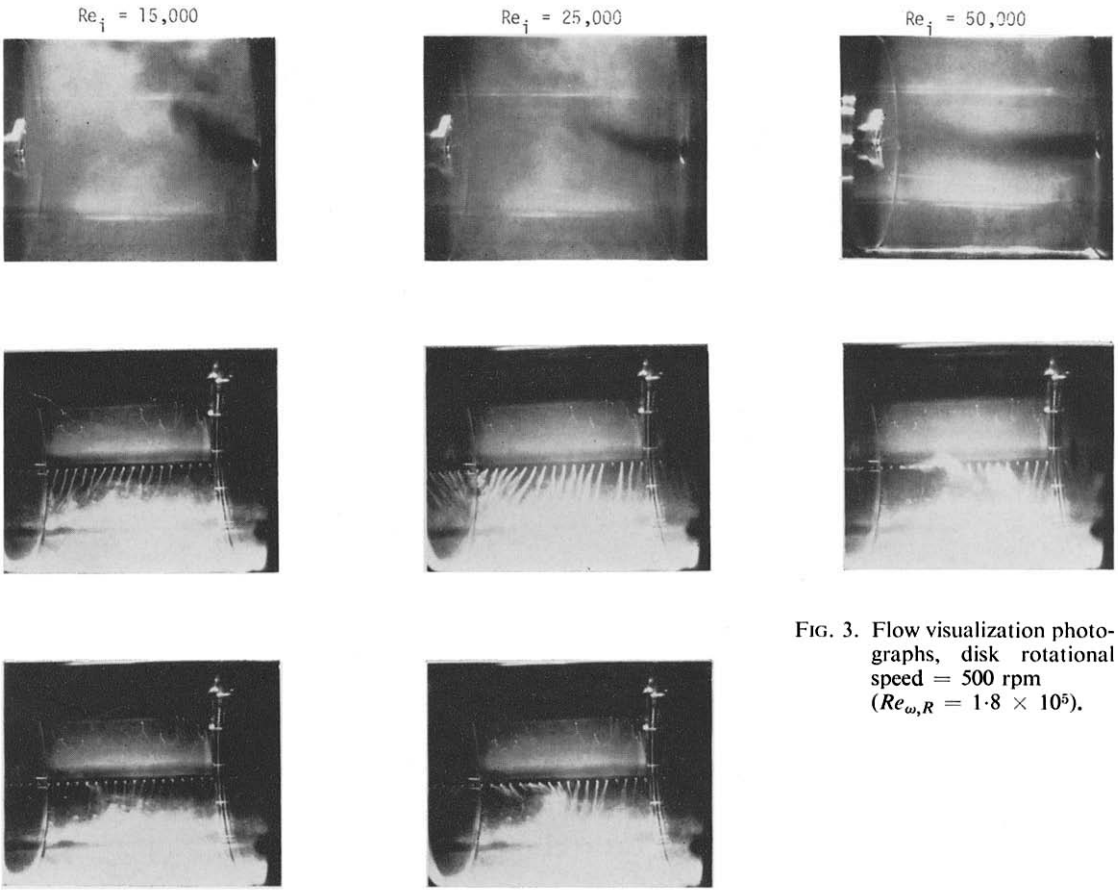

FIG. 3. Flow visualization photographs, disk rotational speed = 500 rpm ($Re_{\omega,R} = 1{\cdot}8 \times 10^5$).

50 000. The upper and middle photographs in the first column and the upper photographs in the second and third columns are views in an illuminated vertical plane which contains the axis of the enclosure. The most prominent feature of the flow patterns for $Re_i = 15\,000$ and 25 000 is the presence of a cone-shaped zone of smoke adjacent to the axis of the cavity. As will be illustrated shortly, this cone corresponds to a region of recirculating flow. The entering coolant is seen to form an annular jet about the smoke cone. At the higher coolant inlet Reynolds number of 50 000, the smoke cone and annular coolant jet are no longer in evidence. Instead, the entering coolant forms a curved cylindrical jet of decreasing diameter. The curved jet revolves about the axis of the enclosure in the same direction as the rotating disk, but at a much lower rotational speed. With the presence of the revolving jet, the flow in the enclosure is no longer axi-symmetric.

For the other photos of Fig. 2, the illumination was focused on the neighborhood of the smoke injection holes in the cylindrical wall. The streams of injected smoke indicate the presence of a strong tangential velocity component and a substantially smaller axial velocity component directed toward the exit of the enclosure. It is the axial velocity component which is responsible for the sloping off of the smoke traces toward the left.

The structure of Fig. 3 (500 rpm) is generally similar to Fig. 2. At 500 rpm, the regime of the revolving jet is already in evidence at the lowest of the Re_i investigated. With increasing values of coolant inlet Reynolds number, the axis of the jet is inclined more and more toward the axis of the enclosure. At $Re_i = 50\,000$, the

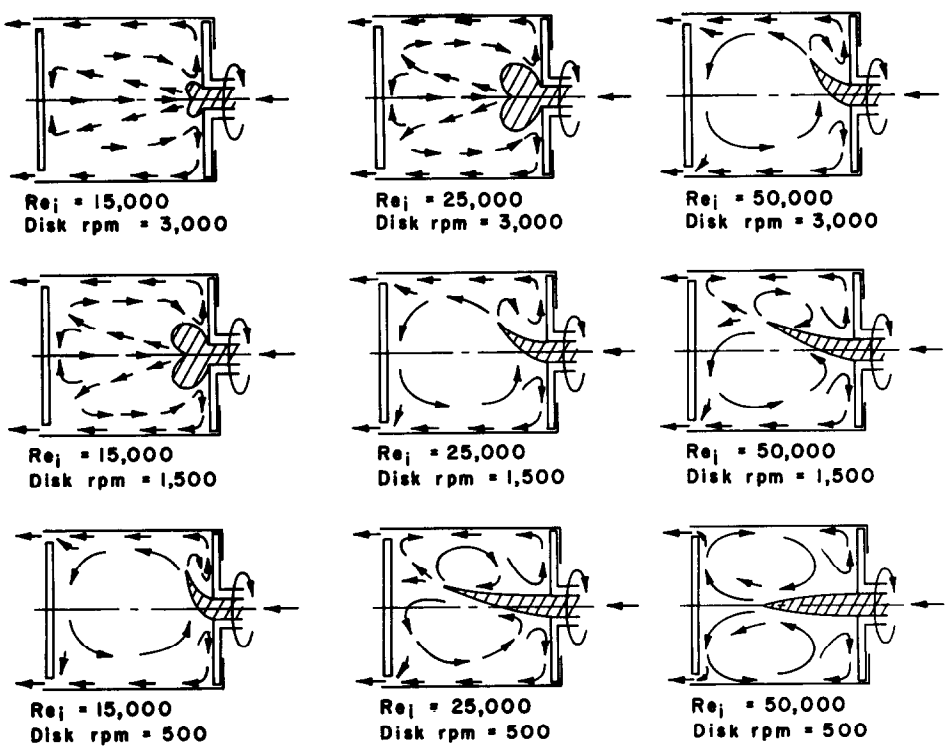

FIG. 4. Flow pattern sketches, spacing to radius ratio = 2.

two axes appear to coincide, so that flow symmetry is restored. The two smoke trace photographs in the first and second columns of Fig. 3 illustrate an interesting effect related to the presence of the revolving jet. In the middle photograph, the axial flow adjacent to the shroud at the downstream end of the enclosure is directed toward the exit, whereas in the lowermost photograph a backflow is in evidence. Thus, as the jet revolves, it creates and carries with it a revolving region of backflow adjacent to the shroud at the downstream end of the enclosure.

The information contained in Figs. 2 and 3 was supplemented by many hours of direct visual observations of the smoke patterns. On the basis of these observations, sketches of the flow patterns were prepared and are presented in Figs. 4–6, respectively, for spacing to radius ratios s/R of 2, 0·89 and 0·44.

Figure 4 summarizes the main features of the photographs of Figs. 2 and 3 and provides additional information not available in the photographs. The first, second, and third rows of sketches correspond, respectively, to rotational speeds of 3000, 1500 and 500 rpm. The coolant inlet Reynolds number Re_i increases from left to right in each row.

Inspection of the figure suggests that a qualitative correlation for the flow regimes can be made in terms of the ratio of Re_i to the disk rotational speed. For the smaller values of this parameter, the flow is axi-symmetric, with a conical recirculation zone adjacent to the axis and an annular coolant jet. For larger values, the coolant forms a revolving cylindrical jet

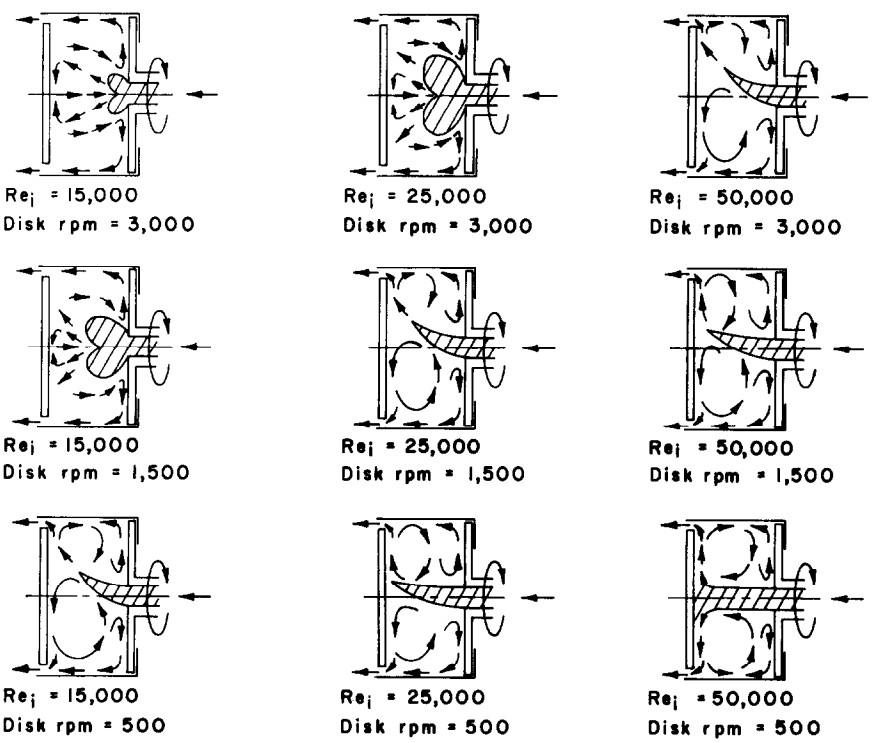

FIG. 5. Flow pattern sketches, spacing to radius ratio = 0·89.

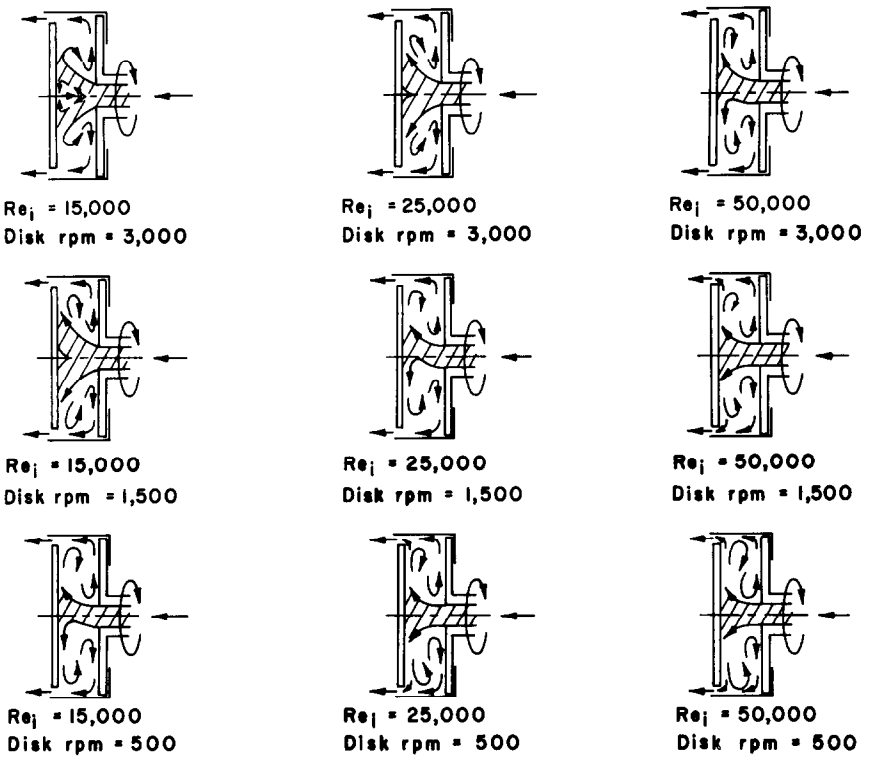

FIG. 6. Flow pattern sketches, spacing to radius ratio = 0·44.

whose axis is inclined more and more toward the axis of the enclosure as the ratio increases. Finally, the axes of the jet and the enclosure coincide, and axi-symmetric conditions are restored. Backflows along the shroud at the downstream end of the enclosure are in evidence in all but the first of the flow regimes.

Flow field sketches for a spacing to radius ratio s/R of 0·89 are presented in Fig. 5. The flow patterns and their correlation with the ratio of Re_i to disk rotational speed are the same as for $s/R = 2$. For both values of s/R, the rotational speed of the revolving coolant jet was found to be between 20–30 cycles per min, with no apparent correlation with the speed of the rotating disk.

Corresponding sketches are presented in Fig. 6 for $s/R = 0{\cdot}44$. The previously discussed flow regimes continue to exist, but now, the coolant jet impinges directly on the stationary disk. The backflows along the shroud that were observed for this case appeared stronger than for the larger spacings.

Visualization of the flow field for $s/R = 0{\cdot}22$ was also attempted. The findings were not conclusive because of observation difficulties and because of the very high rates of smoke flow that were necessary to cope with the high velocities attained by the coolant fluid.

In addition to the foregoing, smoke studies were performed to examine the flow in the annular gap between the stationary disk and the shroud. For a given disk rotational speed, it was found that for lower values of Re_i, inflow could occur from the downstream surroundings into the enclosure (see [15] for details). A similar

observation has been made by Bayley and Owen [1] for a different shrouded configuration. There was no such inflow for any of the conditions for which heat transfer results are reported here.

HEAT TRANSFER RESULTS

Local heat transfer coefficients were evaluated from the defining equation

$$h = q/(T_w - T_f). \quad (1)$$

The local heat flux q was found from the measured electric power input plus an accounting of the axial and radial heat conduction. The local wall temperature T_w was measured either by thermistor or thermocouple, respectively on the rotating disk or on the stationary shroud.

tive temperature survey are presented in Fig. 7, which shows time-averaged radial temperature distributions* at various axial stations x, where x is measured from the surface of the rotating disk. As a supplement to the operating conditions noted in the figure, the coolant inlet temperature was 89°F and the shroud surface temperature ranged from 118 to 132°F. Inspection of the figure indicates a rapid drop in the air temperature adjacent to the rotating disk and then a more gradual rise in temperature as x increases. Clearly, the temperature of the air within the enclosure is not sufficiently uniform to permit identification of a free stream temperature.

After consideration of the alternative candidates for T_f, it appeared that the coolant inlet

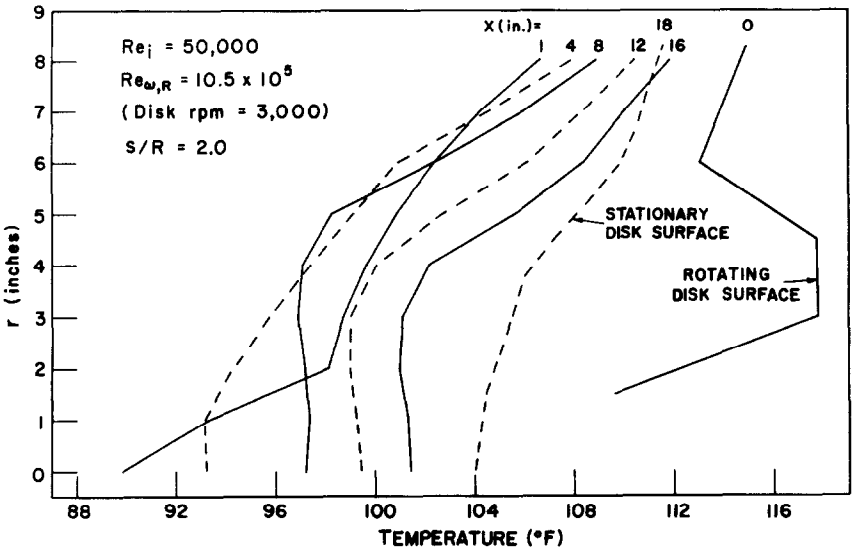

FIG. 7. Representative air temperature distributions in the enclosure.

To complete the evaluation of h, it remains to specify the fluid temperature T_f. In this connection, measurements made with a traversing thermocouple probe indicated that a uniform free stream temperature could not be identified within the enclosure. The results of a representa-

bulk temperature was the best choice since, in applications, this temperature would probably be known (e.g. bleed air temperature). However,

* The unsteadiness of the temperature field presumably resulted from the presence of the rotating, curved coolant jet.

direct measurement of the inlet bulk temperature did not appear practical. First of all, temperature and velocity profile measurements, performed with highly extended probes entering from the downstream end of the enclosure, would have been difficult and subject to uncertainty, especially in rotating flows where probes are washed by their own wakes. Furthermore, owing to rotation, a zone of reverse flow can exist adjacent to the centerline of the coolant inlet pipe, thereby compounding the difficulties of measurement and interpretation. In view of these factors, the inlet bulk temperature was calculated from the coolant exit temperature by means of an energy balance.

The coolant exit temperature itself was found by averaging the outputs of twenty-four thermocouples situated in the exit cross section (see Apparatus section for thermocouple locations). The evaluation of the energy balance to determine the inlet bulk temperature took account of the electric power input to the heaters; conduction heat losses from the rotating disk, the stationary disk, and the shroud; and the work input of the rotating disk. For the work term, the torque correlation of Schultz-Grunow [11] was used as discussed in [15].

The nominal thermal boundary condition of the experiments was uniform surface heat flux, and this was generally fulfilled to within 10 per cent. However, since the heaters for the rotating disk and the shroud were independently adjustable, different levels of uniform heating could be attained on the two surfaces. Tests were undertaken to examine how the results were affected by different levels of heating on the disk and shroud, and Fig. 8 shows some representative findings. The left- and right-hand portions of the figure give local heat transfer coefficients for the rotating disk and for the shroud, respectively. Results are shown for two cases, one in which the local heat fluxes on the disk and shroud were matched, and a second in which the disk heat flux was twice as great as that for the shroud. The figure shows that the effect of the heat flux ratio on the heat transfer coefficients is not too great, about ten per cent for the rotating disk and 20–25 per cent for the shroud. Evidently,

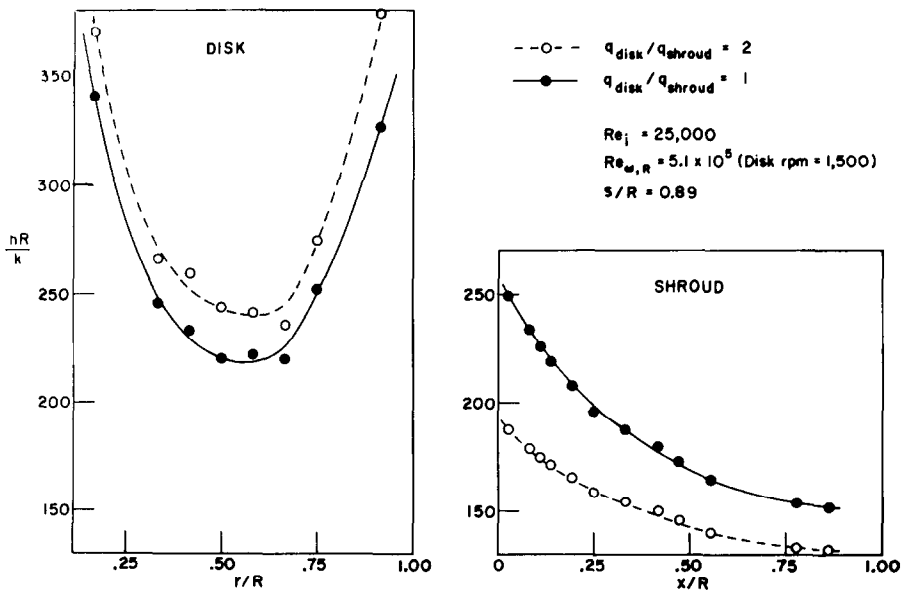

FIG. 8. Effect of different disk and shroud heat flux rates.

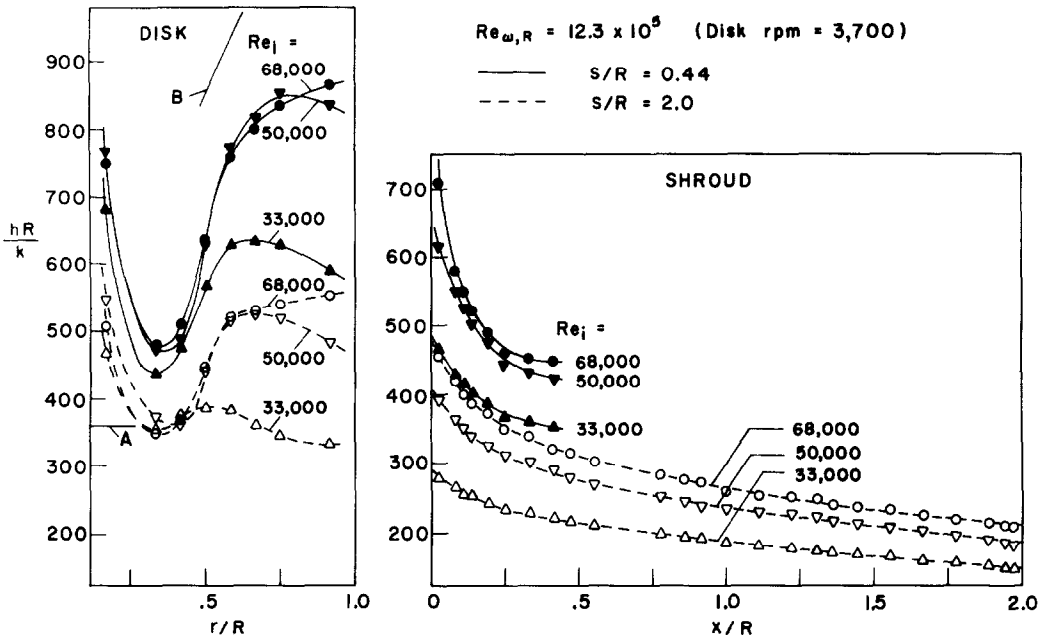

FIG. 9(a). Local heat transfer results, disk rpm = 3700, s/R = 0·44 and 2.

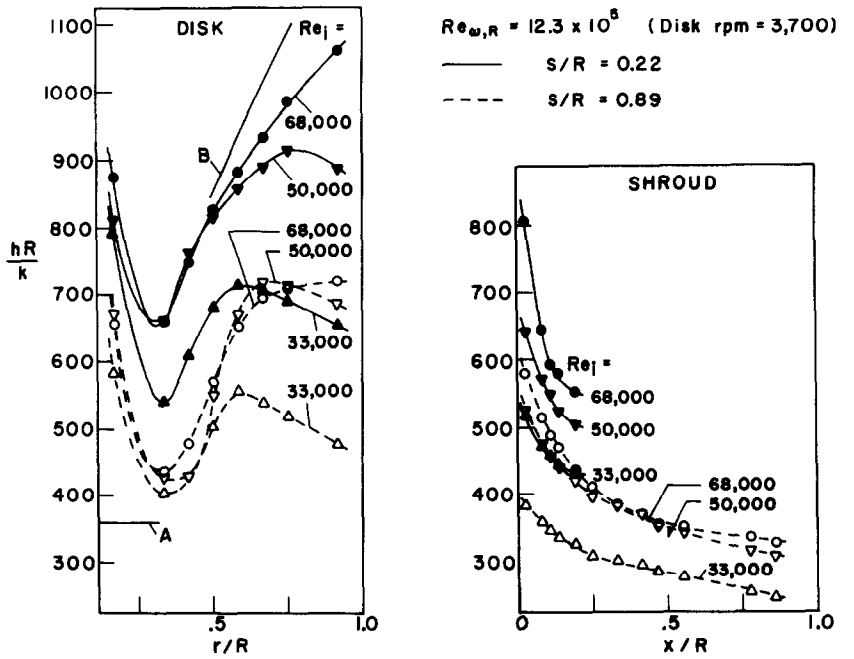

FIG. 9(b). Local heat transfer results, disk rpm = 3700, s/R = 0·22 and 0·89.

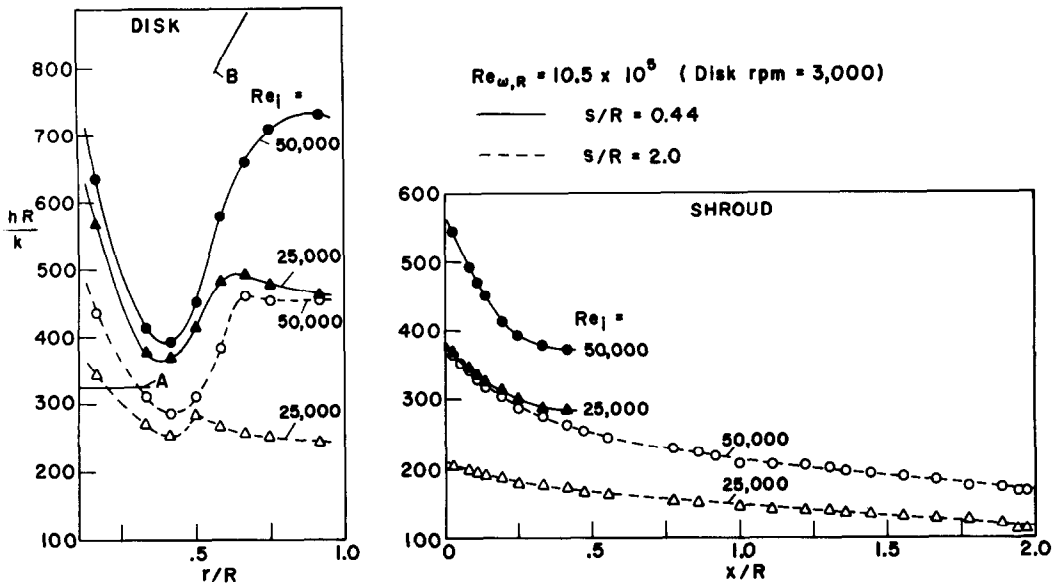

FIG. 10(a). Local heat transfer results, disk rpm = 3000, s/R = 0·44 and 2.

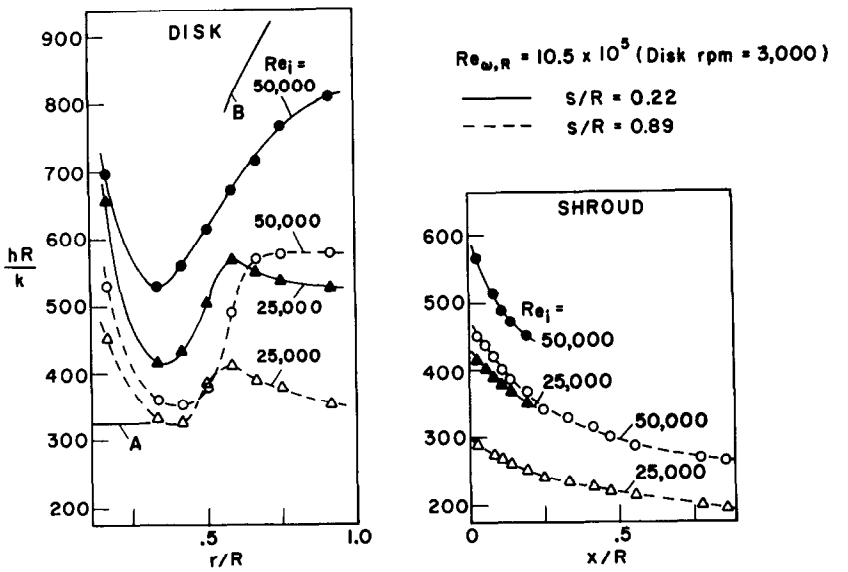

FIG. 10(b). Local heat transfer results, disk rpm = 3000, s/R = 0·22 and 0·89.

small mismatches of q_{disk} and q_{shroud} should have a negligible effect. For all of the data runs to be reported here, the disk and shroud heat fluxes were generally within a few per cent, so that the results may be regarded as corresponding to $q_{\text{disk}}/q_{\text{shroud}} = 1$.

A presentation of local heat transfer results is made in Figs. 9–12, respectively for disk rotational speeds of 3700, 3000, 1500 and 500 rpm. Each figure has an (a) and (b) part. In the (a) part, results are given for spacing to radius ratios s/R of 2 and 0·44, whereas the (b) part gives results for $s/R = 0{\cdot}89$ and 0·22. All of the figures have a common structure. The left-hand portion of the figure contains heat transfer results for the rotating disk, which are plotted against the dimensionless radial coordinate r/R The right-hand portion shows results for the shroud as a function of the dimensionless axial coordinate x/R.

The local heat transfer coefficients are presented in the terms of a Nusselt number hR/k, where R is the radius of the enclosure and k is the thermal conductivity of air evaluated at the mean of the inlet and outlet coolant temperatures.* The coolant inlet Reynolds number Re_i and disk rotational Reynolds number $Re_{\omega,R}$ appear as parameters and are defined as

$$Re_i = 2\dot{m}/\pi\mu R_i, \qquad Re_{\omega,R} = R^2\omega/\nu \tag{2}$$

in which $\dot{m}$ is the coolant flow rate and ω is the rotational speed. The air properties appearing in Re_i and $Re_{\omega,R}$ were respectively evaluated at the inlet and mean bulk temperatures.

Attention may first be turned to the results for 3700 and 3000 rpm, Figs. 9 and 10 respectively. On the rotating disk, the radial distributions of the heat transfer coefficient are seen to decrease at first, reach a minimum, and then increase. Then, depending on the coolant Reynolds number and the spacing, the distribution may attain a maximum and subsequently drop off. This pattern in the surface variation of the heat transfer coefficient is suggestive of laminar, transition, and turbulent flow regimes in the boundary layer adjacent to the rotating disk, and these designations will be used in the subsequent discussion. The results indicate that the heat transfer coefficients are relatively insensitive to the coolant Reynolds number Re_i in the laminar regime; in the turbulent regime, the heat transfer coefficients increase markedly as Re_i increases. Also, higher heat transfer coefficients are in evidence at smaller disk spacings.

In addition to the present experimental results, the rotating disk portions of Figs. 9 and 10 contain lines designated as A and B. These lines correspond, respectively, to laminar and turbulent heat transfer results for a single, unshrouded isothermal rotating disk situated in an otherwise quiescent fluid environment. The equations from which lines A and B were constructed are, respectively,

$$h(\nu/\omega)^{\frac{1}{2}}/k = 0{\cdot}323,$$
$$hr/k = 0{\cdot}01792\,(r^2\omega/\nu)^{0{\cdot}8} \tag{3}$$

as given by [17, 18]. The heat transfer coefficients of equations (3) are based on the temperature difference between the disk surface and the free stream.

In view of differences in geometrical configuration and in the specification of the fluid temperature, there is no basis on which to expect good correlation between the single disk results of equations (3) and those of the present experiments. It is, therefore, interesting to note that the line A consistently falls near the minimum of the present laminar data for the larger disk spacings. On the other hand, line B falls substantially higher than the present turbulent data for the larger spacings and even exhibits a different trend.

The heat transfer coefficients for the shroud, as presented in the right-hand portions of Figs. 9 and 10, decrease monotonically with axial distance. This suggests a growing thermal boundary layer in the absence of flow transitions. In addition, it affirms the absence of strong

* The temperature rise of the air ranged from 10 to 50°F.

backflows adjacent to the shroud at the downstream end of the enclosure (see Figs. 4–6).

The results for the disk rotational speed of 1500 rpm, Fig. 11, display certain interesting differences in detail compared with those discussed above. First of all, the turbulent regime is much less in evidence on the rotating disk. Second, the heat transfer coefficients on the shroud are no longer monotonically decreasing with x in all cases. Rather, at the highest coolant

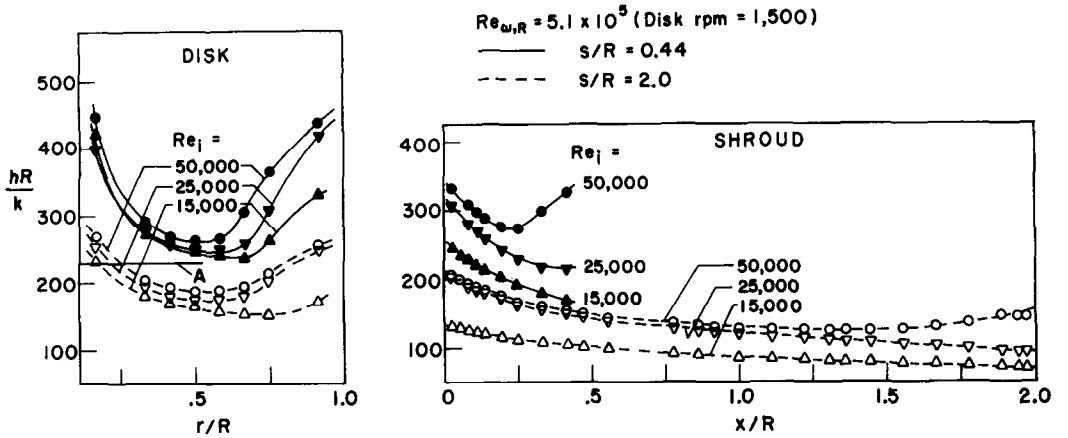

FIG. 11(a). Local heat transfer results, disk rpm = 1500, s/R = 0·44 and 2.

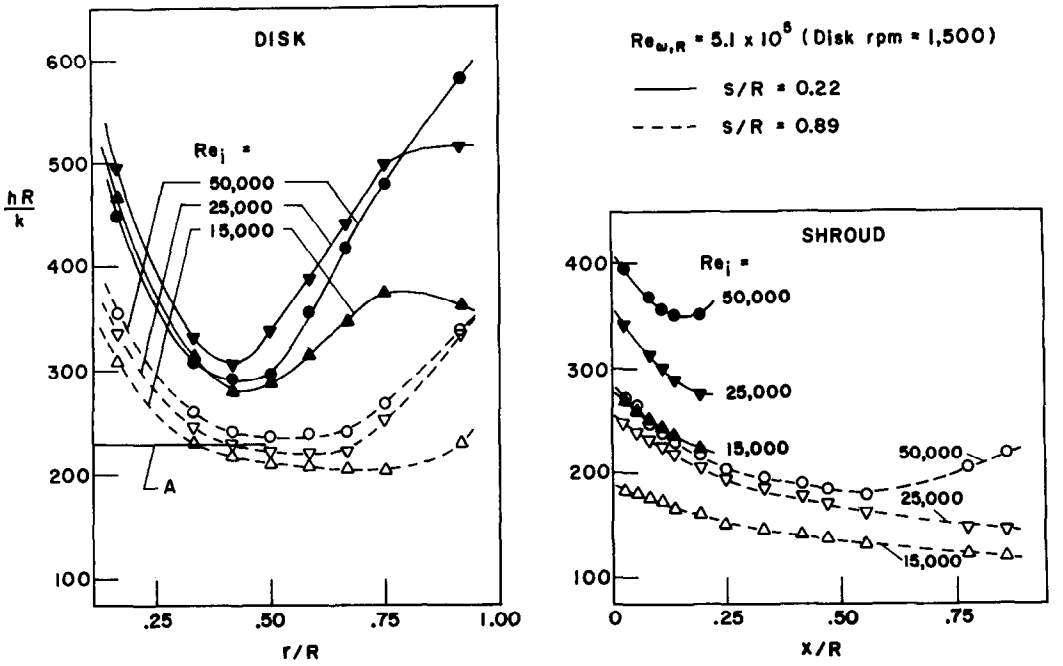

FIG. 11(b). Local heat transfer results, disk rpm = 1500, s/R = 0·22 and 0·89.

Reynolds number of 50 000, the curves tend to increase with x near the downstream end of the enclosure. This trend is attributable to backflow which takes place along the shroud in that region of the enclosure.

At 500 rpm, Fig. 12, substantial portions of the surface of the rotating disk appear to be in the laminar flow regime. At the larger spacings, the laminar heat transfer coefficients are nearly independent of radial position, as is the case for

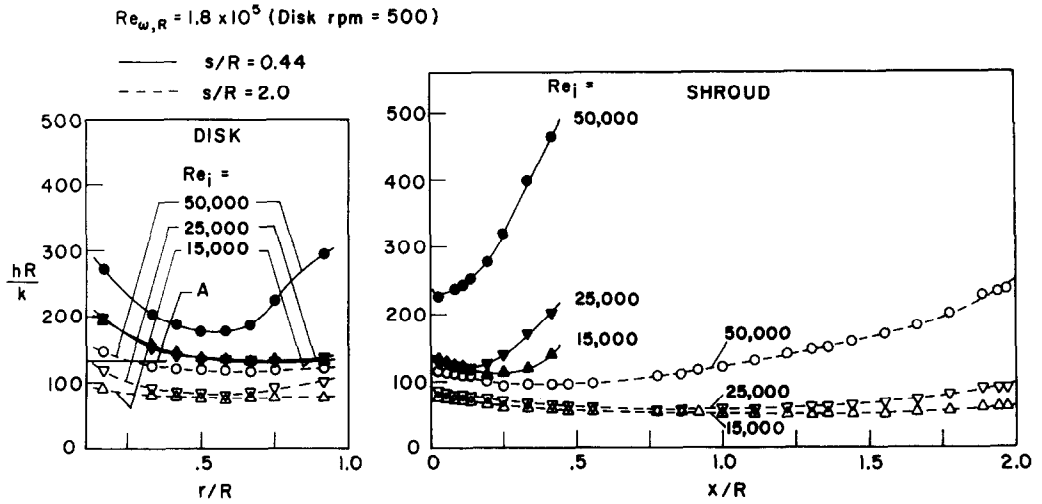

FIG. 12(a). Local heat transfer results, disk rpm = 500, s/R = 0·44 and 2.

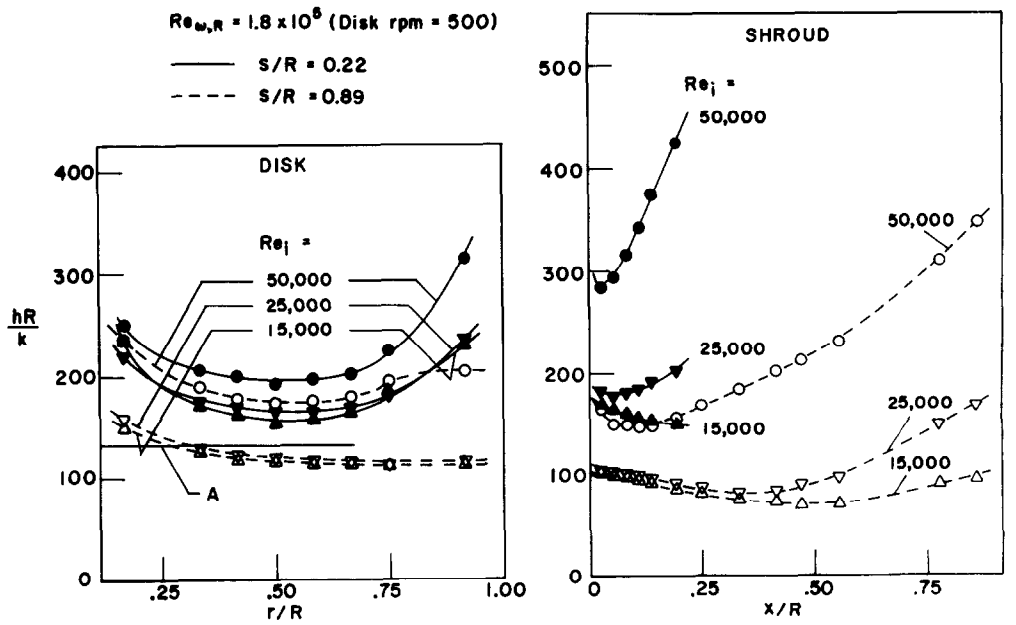

FIG. 12(b). Local heat transfer results, disk rpm = 500, s/R = 0·22 and 0·89.

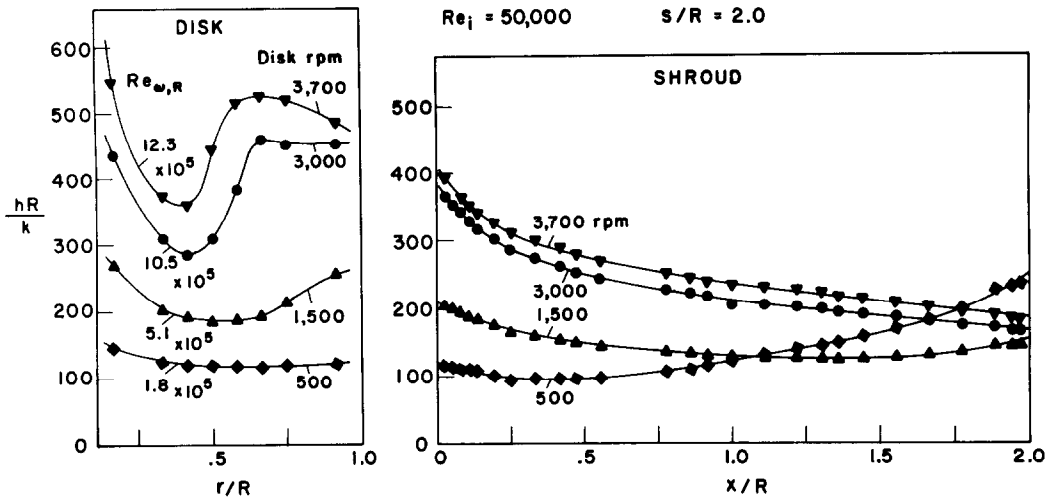

FIG. 13(a). Effect of disk rotational speed on local heat transfer results, spacing to radius ratio = 2.

the single rotating disk (see the first of equations (3)). On the shroud, the curves either initially or ultimately increase with increasing x, a trend which is emphasized at small spacings and large coolant Reynolds numbers, both of which accentuate backflow adjacent to the shroud.

The influence of disk rotational speed on the heat transfer results is highlighted in Figs. 13, which correspond to a fixed coolant flow rate (Re_i = 50 000) and to fixed spacing ratios s/R of 2 ((a) part) and 0·22 ((b) part). Curves are given for rotational speeds of 3700, 3000, 1500 and 500 rpm. On the rotating disk, the heat transfer coefficients are seen to increase with increasing rotational speed. In addition, the flow regime is markedly affected. At the lowest speed, the flow is substantially laminar. With increasing speed, transition occurs at smaller and smaller radii, and turbulence is in evidence at the larger radii. From the results for the shroud, it is evident that significant backflows set in at the lower rotational speeds.

To facilitate interpolations to other operating conditions, correlation equations have been fitted to the local Nusselt number results for the

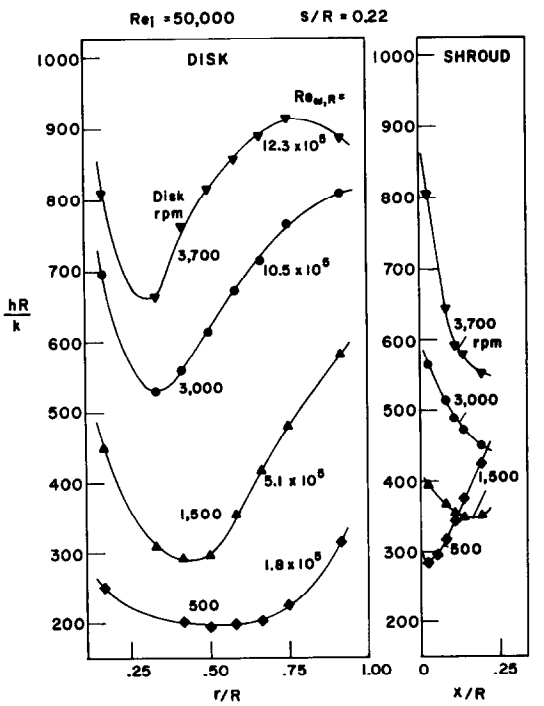

FIG. 13(b). Effect of disk rotational speed on local heat transfer results, spacing to radius ratio = 0·22.

rotating disk. These correlations are given in the Appendix. The laminar correlation extends up to $r^2\omega/\nu = 1{\cdot}5 \times 10^5$, whereas the turbulent correlation applies for $r^2\omega/\nu > 1{\cdot}5 \times 10^5$. It is interesting to note that laminar-turbulent transition for the single rotating disk also occurs in this range. No correlation was attempted for the shroud, owing to the complex trends brought about by backflow.

Average heat transfer coefficients $\bar{h}$ were evaluated for the rotating disk and for the shroud from the defining equation

$$\bar{h} = Q/A(\overline{T_w - T_f}) \tag{4}$$

where Q is the net rate of heat transfer, and $(\overline{T_w - T_f})$ is the surface-averaged temperature difference. The results thus obtained are presented in Fig. 14, with those for the disk plotted in the left-hand portion of the figure and those for the shroud plotted in the right-hand portion. The abscissa variable is the coolant Reynolds number. Each of the separate graphs corresponds to a specific s/R, and the curves are parameterized by the disk rotational speed. The trends in evidence in Fig. 14 are consistent with those already discussed in connection with the local heat transfer results.

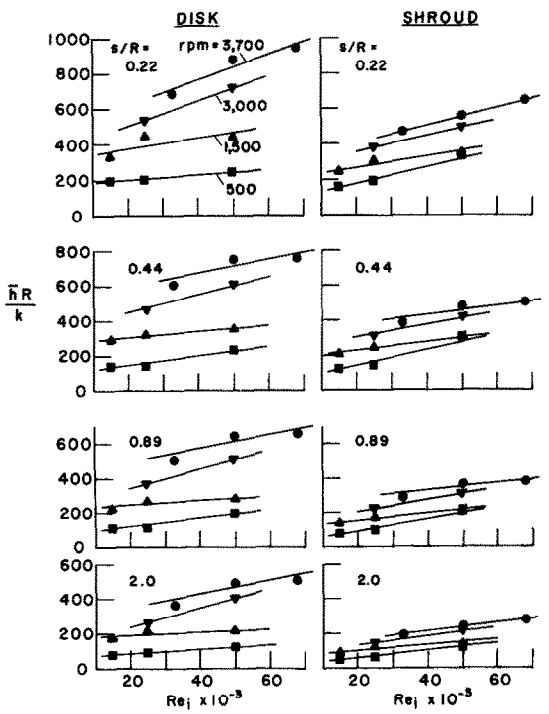

FIG. 14. Average heat transfer coefficients.

CONCLUDING REMARKS

The research described here represents the first reported experimental investigation of the heat transfer characteristics of shrouded, parallel disk systems with rotation and coolant throughflow. The investigation was motivated by cooling problems in cavities and enclosures which may be situated adjacent to the rotating shaft in gas turbines, compressors, and similar devices. The axial and transverse dimension of the present test section were of comparable size, in contrast to the closely spaced disks of prior studies that were concerned with applications involving turbine disks.

Aside from the quantitative heat transfer results presented in the paper, certain qualitative trends may be identified. The local heat transfer coefficients on the rotating disk increase with increasing coolant flow rate, increasing rotational speed, and decreasing spacing between the disks. The shapes of the radial distributions of the transfer coefficients suggest the existence of laminar, transition, and turbulent boundary layers. In the laminar regime, the transfer coefficients are relatively insensitive to the coolant flow rate. Initiation of transition at smaller radii and the existence of the turbulent boundary layer are favored by higher rotational speeds and closer spacings.

The local heat transfer coefficients on the shroud also increase with increasing coolant flow rate and decreasing spacing. Furthermore, at the higher rotational speeds, the transfer coefficients increase with rotational speed. Owing to backflows along the shroud at the lower rotational speeds, the trends are more complex in this range.

Flow visualization, accomplished by injecting smoke into the enclosure, revealed a succession of flow patterns which could be ordered according to the ratio of the coolant inlet Reynolds number to the disk rotational speed.

ACKNOWLEDGEMENT

This research was supported by project N00014-68-A-0141-0001, administered by the Office of Naval Research.

REFERENCES

1. F. J. Bayley and J. M. Owen. The fluid dynamics of a shrouded disk system with radial outflow of coolant. *J. Engng Power* **92**, 335 (1970).
2. D. K. Hennecke, E. M. Sparrow and E. R. G. Eckert. Flow and heat transfer in a rotating enclosure with axial throughflow. *Wärme- und Stoffübertragung* **4**, 222 (1971).
3. T. Vannerus, Rotierende Scheiben für Luftvorwärmer Gebläsewirkung. *Allgem. Wärmetechnik* **6**, 257 (1955).
4. S. L. Soo. Laminar flow over an enclosed rotating disk. *Trans. Am. Soc. Mech. Engrs* **80**, 287 (1958).
5. S. L. Soo, R. W. Besant and Z. N. Sarafa. The nature of heat transfer from an enclosed rotating disk. *Z. Angew. Math. Phys.* **13**, 297 (1962).
6. F. Kreith, E. Doughman and H. Kozlowski. Mass and heat transfer from an enclosed rotating disk with and without source flow. *J. Heat Transfer* **85**, 153 (1963).
7. J. W. Mitchell. A study of the fluid dynamics and heat transfer behavior for radially inward flow over a shrouded rotating disk. Department of Mechanical Engineering, Stanford University, TR No. 57 (1963).
8. V. M. Kapinos. Heat transfer during the flow of a stream from the center to the periphery between two rotating disks. *Int. Chem. Engng* **5**, 461 (1965).
9. F. J. Bayley and J. M. Owen. Flow between a rotating and a stationary disk. *Aero. Quart.* **20**, 333 (1969).
10. J. M. Owen. The effect of forced flow on heat transfer from a disc rotating near a stator. *Int. J. Heat Mass Transfer* **14**, 1135 (1971).
11. F. Schultz-Grunow. Der Reibungswiderstand rotierender Scheiben in Gehäusen. *Z. Angew. Math. Mech.* **15**, 191 (1935).
12. K. G. Picha. An experimental study of the flow between two rotating coaxial disks. Ph.D. Thesis, Department of Mechanical Engineering, University of Minnesota (1957).
13. J. W. Daily and R. E. Nece. Chamber dimension effects on induced flow and frictional resistance of enclosed rotating disks. *J. Basic Engng* **82**, 217 (1960).
14. R. Izumi and A. Iguchi. Mass transfer from the rotating disk to cylinder. *Japan Nat. Cong. Appl. Mech.*, 203 (1965).
15. J. P. Yu. Experiments on flow and heat transfer in a cavity bounded by rotating surfaces. Ph.D. Thesis. Department of Mechanical Engineering, University of Minnesota (1971).
16. J. P. Yu, E. M. Sparrow and E. R. G. Eckert. A smoke generator for use in fluid flow visualization. *Int. J. Heat Mass Transfer* **15**, 557 (1972).
17. E. M. Sparrow and J. L. Gregg. Mass transfer, flow and heat transfer about a rotating disk. *J. Heat Transfer* **82**, 294 (1960).
18. S. T. McComas and J. P. Hartnett. Temperature profiles and heat transfer associated with a single isothermal disk rotating in still air. Paper FC 7.7, Proceedings, Fourth International Heat Transfer Conference, Vol. III (1970).

APPENDIX

Correlations of Local Nusselt Numbers on the Disk

Correlation of the local heat transfer coefficients for the disk was carried out in terms of the following dimensionless parameters:

$$Nu_r = hr/k,\ Re_i = 2\dot{m}/\pi\mu R_i,\ Re_{\omega,r} = r^2\omega/\nu,\ s/R,\ r/R.$$

The laminar correlation, applicable for $Re_{\omega,r} < 1{\cdot}5 \times 10^5$, is given by

$$\begin{aligned}\ln(Nu_r) = &-3{\cdot}753 - 0{\cdot}2415\ln(s/R)\\ &- 0{\cdot}03537[\ln(s/R)]^2 - 0{\cdot}06114\ln(Re_i)\\ &+ 0{\cdot}005728[\ln(Re_i)]^2 + 0{\cdot}8611\ln(Re_{\omega,r})\\ &- 0{\cdot}01243[\ln(Re_{\omega,r})]^2 + 0{\cdot}1309\ln(r/R)\\ &+ 0{\cdot}2897[\ln(r/R)]^2.\end{aligned} \quad (5)$$

In the turbulent range, for $Re_{\omega,r} > 1{\cdot}5 \times 10^5$, a correlation of the data is

$$\begin{aligned}\ln(Nu_r) = &-36{\cdot}71 - 0{\cdot}2999\ln(s/R)\\ &- 0{\cdot}009616[\ln(s/R)]^2 - 0{\cdot}07580\ln(Re_i)\\ &+ 0{\cdot}006869[\ln(Re_i)]^2 + 5{\cdot}686\ln(Re_{\omega,r})\\ &- 0{\cdot}1869[\ln(Re_{\omega,r})]^2 - 0{\cdot}1287\ln(r/R)\\ &+ 0{\cdot}2925[\ln(r/R)]^2.\end{aligned} \quad (6)$$

EXPERIENCES SUR UNE ENCEINTE A DISQUE TOURNANT AVEC ECOULEMENT DE REFROIDISSEMENT

Résumé—On a étudié en présence d'un écoulement de refroidissement les caractéristiques du transfert thermique et de l'écoulement du fluide dans une enceinte cylindrique ayant à la fois des parois en rotation

et des parois fixes. Cette recherche est motivée par les applications du refroidissement dans des cavités et des enceintes qui peuvent être adjacentes à l'arbre mobile dans les turbines à gaz, les compresseurs et des dispositifs similaires. Les parois de la section de mesure consistent en un disque tournant chauffé, une paroi cylindrique fixe chauffée et un disque fixe isolé. Le réfrigérant qui s'écoule à travers l'enceinte est de l'air. Les expériences sont conduites pour différentes vitesses de rotation du disque, différents débits de réfrigérant et plusieurs espacements entre les disques.

On trouve que les coefficients locaux de transfert thermique sur le disque tournant croissent quand la vitesse de rotation et le flux du réfrigérant augmentent et lorsque diminue l'espacement. Les formes des distributions radiales des coefficients de transfert suggèrent l'existence des régimes laminaires, transitoires et turbulents. Dans le régime laminaire, les coefficients de transfert sont relativement insensibles au débit du réfrigérant. Pour l'enveloppe, les comportements en liaison avec la vitesse de rotation, l'écoulement du réfrigérant et l'espacement sont généralement semblables à ceux relatifs au disque tournant. Cependant, étant donnés les écoulements de retour le long de l'enveloppe aux vitesses de rotation les plus basses, les comportements deviennent plus complexes. La visualisation de l'écoulement par injection de fumée, révèle une succession de configurations d'écoulement qui peut être ordonnée selon le rapport de la vitesse du réfrigérant à la vitesse de rotation du disque.

VERSUCHE AN EINEM SYSTEM UMMANTELTER, PARALLELER KREISSCHEIBEN MIT ROTATION UND KÜHLMITTELDURCHFLUSS

Zusammenfassung—Der Wärmeübergang und die Strömungscharakteristik in einem zylindrischen Hohlraum mit sowohl rotierenden als auch stationären Wänden wurde bei der Durchströmung eines Kühlmittels untersucht. Die Untersuchung war motiviert durch Kühlanordnungen in Form von Hohlräumen, in rotierenden Wellen von Gasturbinen, Kompressoren und anderen ähnlichen Apparaten. Die Wände des Versuchsteiles bestanden aus einer beheizten, rotierenden Kreisscheibe, einer beheizten, stationären zylindrischen Ummantelung und einer isolierten, stationären Kreisscheibe. Das den Hohlraum durchströmende Kühlmittel war Luft. Bei den Experimenten wurden Rotationsgeschwindigkeit, Durchfluss des Kühlmittels und Zwischenraum der Scheiben variiert.

Es zeigte sich, dass der lokale Wärmeübergangskoeffizient ansteigt mit steigender Rotationsgeschwindigkeit, wachsendem Kühlmitteldurchfluss und verringertem Zwischenraum. Die Formen der radialen Verteilungen des Wärmeübergangskoeffizienten lassen auf die Existenz laminarer Übergangsgebiete und turbulenter Bereiche schliessen. Im laminaren Bereich waren die Wärmeübergangskoeffizienten relativ unempfindlich gegen die Grösse des Kühlmitteldurchflusses. Bei der Ummantelung zeigten sich in der Abhängigkeit von Rotationsgeschwindigkeit, Kühlmitteldurchfluss und Zwischenraum ähnliche Tendenzen wie bei der rotierenden Scheibe. Sie waren Jedoch in diesem Bereich aufgrund von Rückströmungen längs der Ummantelung bei niedrigeren Rotationsgeschwindigkeiten komplexer. Die durch Einblasen von Rauch sichtbar gemachte Strömung zeigt eine Aufeinanderfolge von Strömungsformen, die aus dem Verhältnis von Kühlmitteldurchfluss zu Rotationsgeschwindigkeit erklärt werden kann.

ЭКСПЕРИМЕНТАЛЬНОЕ ИССЛЕДОВАНИЕ СИСТЕМЫ ЗАКРЫТЫХ ПАРАЛЛЕЛЬНЫХ ДИСКОВ ПРИ ВРАЩЕНИИ И СКВОЗНОМ ОХЛАЖДЕНИИ

Аннотация—Исследовались теплообменные и гидродинамические характеристики цилиндрических камер с вращающимися и неподвижными ст стенками при вдуве охладителя. Исследование связано с задачами охлаждения в полостях и кожухах, примыкающих к вращающемуся валу, в газовых турбинах, компрессорах и аналогичных устройствах. Стенками рабочего участка служили нагретый вращающийся диск, нагретый вращающийся кожух и изолированный неподвижный диск. Через цилиндр продувался воздух-охладитель. Опыты проводились при различных скоростях вращения диска, расходах охладителя и расстояниях между дисками.

Найдено, что локальные коэффициенты теплообмена для вращающегося диска увеличиваются с увеличением скорости вращения, расхода охладителя и расстояний между дисками. Профили радиального распределения коэффициентов переноса свидетельствуют о существовании ламинарного, переходного и турбулентного режимов. При ламинарном режиме коэффициенты переноса не чувствительны у расходу охладителя. Для кожуха наблюдались те же зависимости теплообмена от скорости вращения, расхода охладителя и расстояния, что и для вращающегося диска. Однако из-за вторичных течений вдоль кожуха, возникающих при более низких скоростях вращения, эти зависимости более сложные. Дымовая визуализация потока позволила обнаружить последовательность режимов течения, которые можно систематизировать по отношению расхода охлдителя к скорости вращения диска.